Title

Nanoporous Polymer Films with a High Cation Transference Number Stabilize Lithium Metal Anodes in Light-Weight Batteries for Electrified Transportation

Journal

Nano Letters, 19(2)

ISSN

1530-6984

Authors

Ma, Lin

Fu, Chengyin

Li, Longjun

et al.

Publication Date

2019-02-13

DOI

10.1021/acs.nanolett.8b05101

Peer reviewed

Nanoporous Polymer Films with a High Cation Transference Number Stabilize Lithium Metal Anodes in Light-Weight Batteries for Electrified Transportation

Lin Ma,[†] Chengyin Fu,[‡] Longjun Li,[†] Karthik S. Mayilvahanan,[§] Tylan Watkins,[∥,⊥] Brian R. Perdue,[⊥,#] Kevin R. Zavadil,[∥,⊥] and Brett A. Helms[*,†,‡,¶]

[†]Joint Center for Energy Storage Research, Lawrence Berkeley National Laboratory, 1 Cyclotron Road, Berkeley, California 94720 United States

[‡]The Molecular Foundry, Lawrence Berkeley National Laboratory, 1 Cyclotron Road, Berkeley, California 94720, United States

[§]Department of Chemical and Biochemical Engineering, University of California, Berkeley, California 94720, United States

[∥]Material, Physical, and Chemical Sciences Center, Sandia National Laboratories, P.O. Box 5800, Albuquerque, New Mexico 87185, United States

[⊥]Joint Center for Energy Storage Research, Sandia National Laboratories, P.O. Box 5800, Albuquerque, New Mexico 87185, United States

[#]Power Sources Technology Group, Sandia National Laboratories, Albuquerque, New Mexico 87158, United States

[¶]Materials Sciences Division, Lawrence Berkeley National Laboratory, 1 Cyclotron Road, Berkeley, California 94720, United States

ABSTRACT: To suppress dendrite formation in lithium metal batteries, high cation transference number electrolytes that reduce electrode polarization are highly desirable, but rarely available using conventional liquid electrolytes. Here, we show that liquid electrolytes increase their cation transference numbers (e.g., ~0.2 to >0.70) when confined to a structurally rigid polymer host whose pores are on a similar length scale (0.5−2 nm) as the Debye screening length in the electrolyte, which results in a diffuse electrolyte double layer at the polymer−electrolyte interface that retains counterions and reject co-ions from the electrolyte due to their larger size. Lithium anodes coated with ~1 μm thick overlayers of the polymer host exhibit both a low area-specific resistance and clear dendrite-suppressing character, as evident from their performance in Li−Li and Li−Cu cells as well as in post-mortem analysis of the anode's morphology after cycling. High areal capacity Li−S cells (4.9 mg cm^{-2}; 8.2 mAh cm^{-2}) implementing these high transference number polymer-hosted liquid electrolytes were remarkably stable, considering ~24 μm of lithium was electroreversibly deposited in each cycle at a C-rate of 0.2. We further identified a scalable manufacturing path for these polymer-coated lithium electrodes, which are drop-in components for lithium metal battery manufacturing.

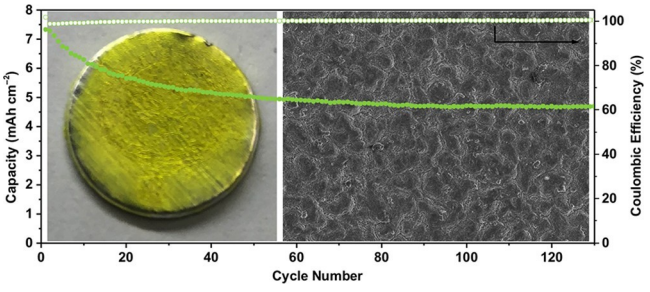

KEYWORDS: *High cation transference number, nanoionics, polymer electrolyte, lithium anode protection, lithium−sulfur battery, electrified transportation*

The electrification of long-haul trucking and flight requires batteries with a higher specific energy density than what is possible with today's lithium-ion batteries, or even next-generation lithium metal batteries with intercalation cath- odes.[1−6] To meet the stringent design specifications for these applications, lithium metal cells employing either oxygen or sulfur cathodes are principally well-positioned (Figure 1A); however, the short cycle life of these cells remains a concern given industry expectations for the battery's service life.[7−10] At the heart of this concern is the chemical and dimensional instability of the lithium metal anode during high-rate electroplating, where dendrite formation is rampant.[11−16] To delay the nucleation and growth of lithium metal

dendrites

while charging the cell, high cation transference number electrolytes are highly desirable to avoid concentration gradients in the cell, but presently out of reach using conventional liquid electrolytes.[12−26]

Here, we show that by confining liquid electrolytes to a 3D network of 0.5−2 nm pores in a microporous polymer overlayer[27] (tunable thicknesses of 0.5−10 μm) on lithium metal, the steady-state cation transference number increases

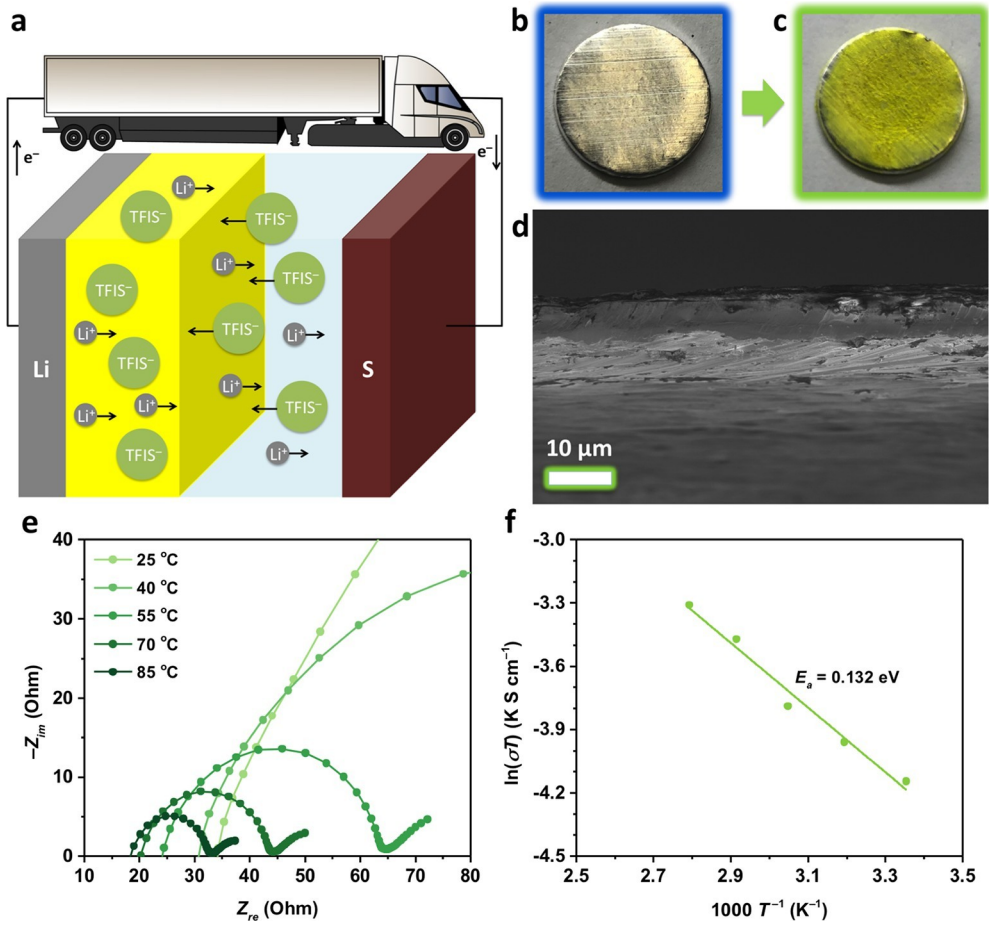

Figure 1. (a) High transference number hybrid electrolytes, comprised of liquid electrolytes confined to nanoporous polymers, on Li anodes reduce Li−S cell polarization at high C-rates, allowing Li metal to be uniformly electroplated with dense morphologies, which reduces the likelihood for dendrite formation. A comparison of (b) bare and (c) PIM-1-coated Li electrodes. (d) Cross-sectional scanning electron micrograph of the Li electrode with the PIM-1 overlayer. (e) EIS spectra of Li−Li symmetric cells, where each electrode is a PIM-1-coated electrode, taken at different temperatures. (f) Arrhenius plot used to extract the activation energy (E_a) for ionic conductivity (σ) within the PIM-1 overlayer infiltrated with 1.0 M LiTFSI in 1:1 DOL/DME (v/v).

from t^+_{ss} = 0.2−0.4 in the bulk electrolyte[28] to t^+ = 0.72 in the nanoconfined polymer electrolyte (Figure 1B−F). Consistent with theoretical predictions for high cation transference number electrolytes,[29] we significantly delay the onset of shorting behavior associated with dendrite formation in lithium−metal cells: from 240 to 750 h in Li−Li symmetric cells cycled at 1 mA cm^{-2}, where 1 mAh of Li is (de)plated in each cycle, and from 14 to 25 h in asymmetric Li−Cu cells under continuous plating at 2 mA cm^{-2}. We further apply these dimensionally stable, polymer-coated Li electrodes in high areal capacity Li−S cells[30] (8.2 mAh cm^{-2}; 4.9 mg cm^{-2}) to extend their cycle life, where the accessed capacity stabilizes at ~960 mAh g^{-1} (~4.7 mAh cm^{-2}) over 120 cycles at 0.2 C. We also identify a manufacturing route to large-area polymer-coated lithium electrodes, which takes advantage of the polymer's preferential adhesion to Li compared to polyolefins. In our scheme, the polymer is applied at a desired thickness from concentrated ink onto a low-cost (~$1/m^2) porous polyolefin film. This hybrid is then pressure-laminated to the Li electrode and the polyolefin layer peeled away to reveal the polymer-coated Li electrode. Such a component is likely to be useful for battery manufacturing and may protect Li from adventitious surface reactions.

Our work points to new opportunities to advance and apply precisely architected, structurally rigid macromolecular materi- als to study the role subnanometer nanoconfinement plays in the foundational ion transport properties of polymer electro- lytes for anode stabilization in lithium metal batteries.

Specifically, our microporous ladder polymer host, a polymer of intrinsic microporosity (PIM),[27,31−34] sequesters ions from the electrolyte in a network of pores that is on the same length scale as the Debye screening length in the bulk electrolyte.

This results in a diffuse electrolyte double layer at the polymer−electrolyte interface that likely retains counterions and may even reject co-ions from the electrolyte due to their larger size. In that Li^+ is the smallest ion in the pore network and has few explicit interactions with the microstructured polymer host, its diffusion in the pore network is higher than that of the anion. As a result, the cation transference number increases significantly. With this comes a reduction in cell polarization during lithium metal electroplating. The homog- enization of ion current during electroplating (i.e., the manifestation of ionic rectification with nanostructured hybrid electrolytes) slows the kinetics associated with both the nucleation and growth of lithium metal dendrites. Dendrite suppression by this mechanism is anticipated to extend the cycle life of lithium metal anodes and cells.

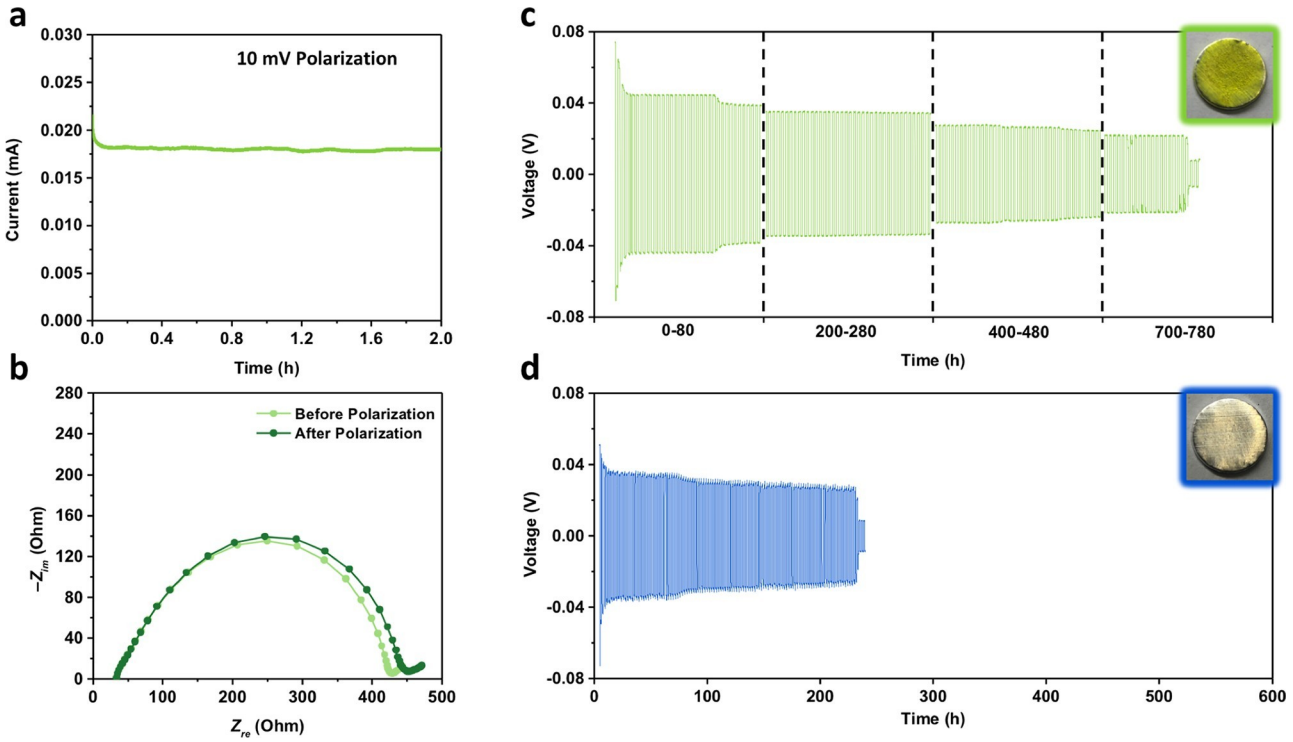

Figure 2. (a) Steady-state current under 10 mV polarization for Li−Li symmetric cells, where each electrode is coated with PIM-1. (b) EIS spectra before and after Li−Li cell polarization. Galvanostatic cycling of Li−Li cells at 1 mA cm^{-2} with a capacity of 1 mAh cm^{-2} at 20 °C, either with (c) or without (d) the PIM-1 overlayer on the Li electrodes. Dashed vertical lines in panel c indicate breaks between data not shown over the cell's full cycling history: specifically, hours 81−199, 281−399, and 481−699. In both panel c and panel d, the plating overpotential gradually decreases over time before shorting is observed. Step changes at the dotted vertical lines in panel c are artifacts of truncating the data series.

Previously reported nanoporous hosts featured pores larger than the Debye screening length; nonetheless, the scaling relationships associated with engineering the electrolyte's transport properties via nanostructuring were firmly estab- lished, providing the motivation for the present study to configure the electrolyte's host to even smaller pore dimensions in a polymer host.[35−38] The collective wisdom from our work in concert with that of others, which now spans several materials classes, confinement length scales, and electrolyte formulations, is that ionic rectification[39−43] in nanoconfined hybrid electrolytes is a powerful strategy to kinetically stabilize lithium metal anodes via dendrite suppression. This is a compelling counterpoint to more traditional means based on high modulus ceramic and block copolymer electrolytes for dendrite blocking, artificial solid-electrolyte interphases (e.g., as generated from lithium nitrate, lithium halides,[44,45] lithium sulfides, cesium or rubidium cations,[46] dual-salt systems,[47−49] etc.), and inorganic glasses[50−52] (e.g., LPS, LGPS, etc.). Furthermore, the ease in which our micro- structured PIM overlayers are applied to the lithium metal electrode surface, either directly from inks or indirectly using our lamination and lift-off sequence, suggests attractive paths forward for lithium metal anode technology development using well-established and low-cost roll-to-roll manufacturing techniques.

To ascertain the extent to which the cation transference number of a liquid electrolyte increases when confined to the 0.5−2 nm pores yielded a 10 μm thick overlayer. The transference number was determined in a symmetric Li−Li cell with 1.0 M LiTFSI and 0.2 M $LiNO_3$ in 1,3-dioxolane (DOL) and 1,2-dimethoxy- ethane (DME) (1:1 v/v) as an electrolyte and Celgard 2400 separating the electrodes. The cell was initially conditioned in order to establish a stable interface between the Li electrode and the polymer; this consisted of charge and discharge cycles at 0.01 mA cm^{-2}. The sequence performed included a 4 h charge, a 30 min rest, a 4 h discharge, and a 30 min rest; this sequence was repeated for a total of 6 times. The cell was then polarized at 10 mV for 10 h (Figure 2A) to ensure steady state was reached; Figure 2B shows the EIS spectra before polarization and after steady-state had been reached. We then calculated the steady-state cation transference number using the method of Bruce and Vincent (eq 1):[53]

$$t^{+}_{ss} = \frac{I_{ss}(\Delta V - I_0 R_0)}{I_0(\Delta V - I_{ss} R_{ss})} \quad (1)$$

where

of a PIM-based polymer host (BET surface area 800 m^2 g^{-1}),[27,31−34] we coated a lithium metal electrode with a solution of PIM-1 in THF (12.5 mg mL^{-1}), which

the applied voltage, I_0 is the initial current, I_{ss} is the steady-state current, R_0 is the initial interfacial resistance, and R_{ss} is the steady-state interfacial resistance. The calculated result shows that PIM-coated lithium electrodes exhibit a high steady-state cation transference number, t_s^+ = 0.72 ± 0.02, which is demonstrably higher, as predicted, than that of the bulk liquid electrolyte, which is 0.2−0.4.[28]

Based on the high steady-state cation transference number of the ethereal electrolyte confined to the PIM-1 host, it is predicted that polarization during electroplating should be significantly reduced due to ionic rectification. Delaying the nucleation and growth of dendrites by this mechanism should

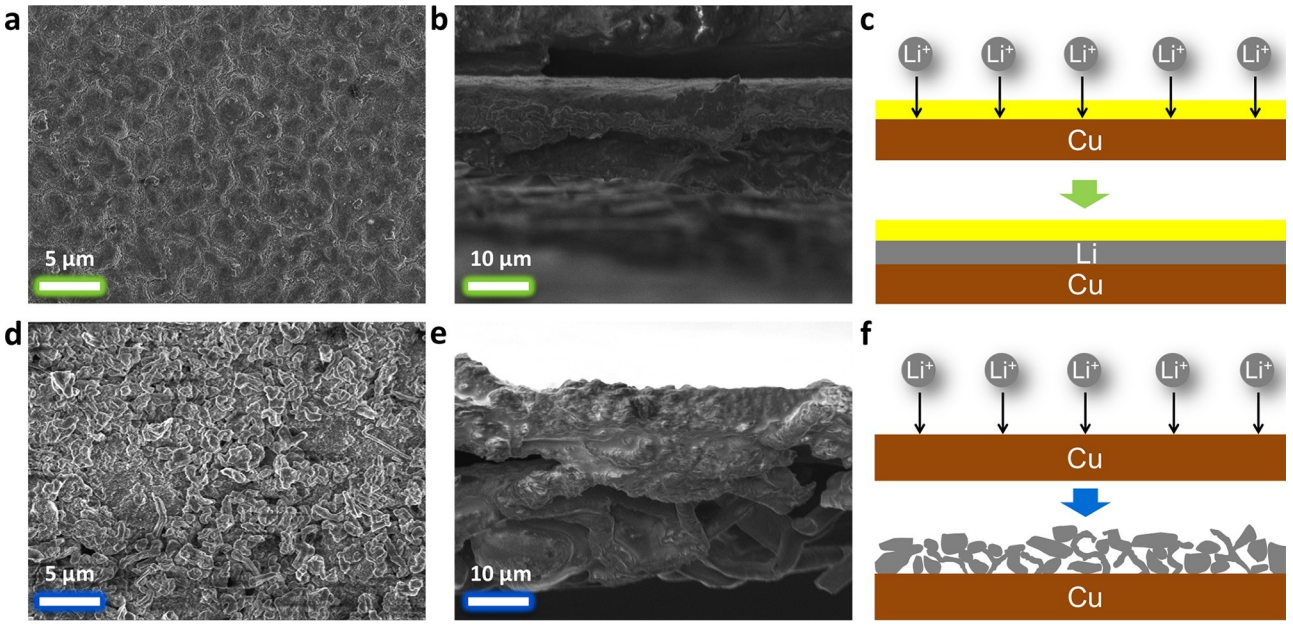

Figure 3. (a) Top-down and (b) cross-sectional analysis by SEM of Li electrodeposits on a PIM-coated Cu electrode, which had been extracted from a Li−Cu cell after 10 cycles at 1 mA cm^{-2} with a capacity of 1 mAh cm^{-2} at 20 °C. For the cross-sectional view, Cu−Li−PIM is visualized from top-to-bottom. (c) Schematic illustration of uniformly dense Li electrodeposits possible with a PIM-1 overlayer; the dashed, green line represents the initial state of the electrode, prior to electrodeposition. (d) Top-down and (e) cross-sectional analysis by SEM of Li electrodeposits on a bare Cu electrode, which has been extracted from a Li−Cu cell cycled under the same conditions. For the cross-sectional view, Cu and Li are visualized from top-to-bottom. (f) Schematic illustration of anisotropic, low density Li electrodeposits observed for liquid-coupled plating; the dashed, blue line represents the initial state of the electrode, prior to electrodeposition.

extend the cycle life of lithium metal anodes. To test this hypothesis, the same symmetric cells were assembled with either PIM-coated or bare lithium electrodes, and the number of cycles prior to cell-shorting failure was determined. The cells were galvanostatically cycled at a current density of 1 mA cm^{-2} and 1 mAh capacity of Li metal plated (or stripped) in each cycle (~5 µm) until the cell shorted, as evidenced by an instantaneous drop in the voltage (Figure 2C,D); while a voltage drop to zero would indicate a hard short, a step-change voltage drop is often attributed to a soft short.[11] This cycling protocol ensures that the amount of lithium moved in a given cycle is sufficient to generate dendrites large enough to short- circuit the cell, unless effectively suppressed by the polymer overlayer at the lithium metal surface.[54]

For Li−Li symmetric cells configured with PIM overlayers (Figure 2C), the cycle life was more than 750 h (total capacity of Li metal plated/deplated = 0.75 Ah); the failure of the cell was attributed to a soft short, in that the voltage drop did not go to zero. Contrasting this behavior, Li−Li symmetric cells without the PIM overlayer evidenced soft shorts after ~250 h of plating and deplating (total capacity of Li metal plated/deplated = 0.25 Ah) (Figure 2D). In both cases, we observed a gradual decrease in the area-specific resistance (ASR) throughout cycling. For Li−Li cells configured with the PIM overlayer, the initial ASR was 60 Ω cm^2 and the rate of ASR withering was 0.0015% per cycle; an ASR of 25 Ω cm^2 was recorded in advance of the soft short. For the control cells, absent the polymer overlayer, the initial ASR was 60 Ω cm^2 and the rate of ASR reduction was 0.0042% per cycle; just prior to the soft short, the ASR was 30 Ω cm^2. The decrease in ASR over time in both cells is attributed to the increase in the surface area of lithium as ramified morphologies manifest over time. Slower ramification of Li deposits in cells configured with the PIM overlayer is notable and consistent with our

hypothesis that high cation transference number electrolytes should suppress dendrite nucleation and growth. This analysis would suggest that lithium metal electrodeposits should be more uniform and dense for electrodes coated with the PIM overlayer than for bare electrodes.

To characterize the morphology of lithium metal electro- deposits on the electrode in the presence or absence of the PIM overlayer, we assembled Li−Cu asymmetric cells where the Cu electrode was either coated or left unmodified. These cells were cycled for 10 cycles at 1 mA cm^{-2}, while 1 mAh capacity of lithium moved in each plate and strip step (i.e., as described above for Li−Li symmetric cells). Terminating in a plate step, the Cu electrode was harvested and imaged top- down and in cross section using scanning electron microscopy (SEM) (Figure 3). In the cell configured with the PIM overlayer, the surface of the Li metal electrodeposit was smooth (Figure 3A), and notably more so compared to the control, where the PIM overlayer was absent (Figure 3D). Further insights into differences in the ramified character of Li metal electrodeposits were gleaned from the cross-sectional SEM views, where dense Li was observed only on Cu coated with the PIM overlayer (Figure 3B,C); nonuniform, highly anisotropic Li metal electrodeposits, which are early signs of dendritic growth, were observed on bare Cu (Figure 3E,F), as expected. Our structural characterization of the electrodeposits provides further support that the high cation transference number PIM electrolyte overlayer improves the uniformity of Li electrodeposition, and, in stride, suppresses lithium dendrite formation at a high rate over long cycling times and large quantities of Li moved per cycle.

Given the dense nature of Li metal electrodeposits when plated through the PIM electrolyte overlayer, we endeavored to understand the influence of lithium metal deposition rate (i.e., current density) on the short-circuit time. Based on the

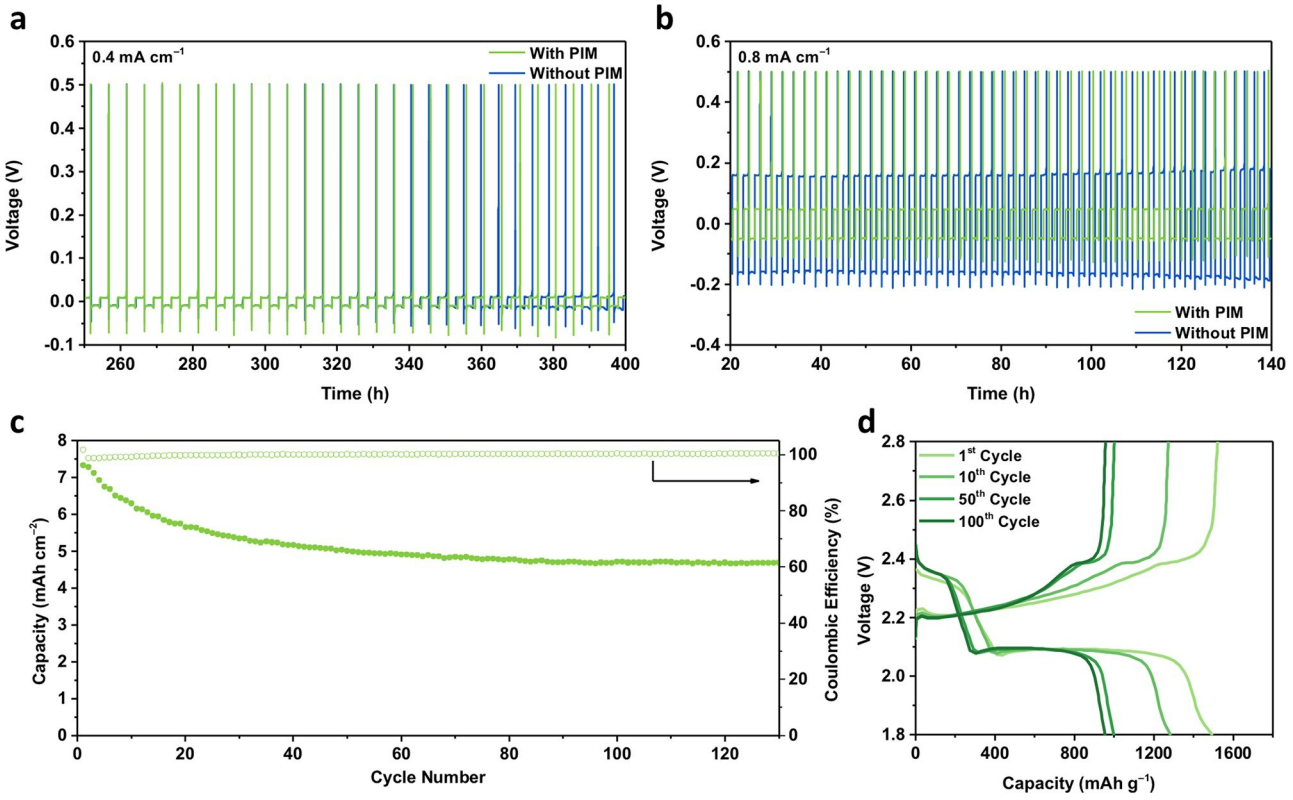

Figure 4. Voltage profile of PIM-modified (green) and unmodified (blue) Li−Cu cells undergoing full plate−strip tests at current densities of either (a) 0.4 mA cm^{-2} and (b) 0.8 mA cm^{-2}. (c) Capacity fade and Coulombic efficiency for high areal capacity Li−S cells cycled at 0.2 C, where the Li anode incorporates the dendrite-suppressing high cation transference number PIM-1 overlayer. (d) Galvanostatic charge−discharge curves of a high areal capacity Li−S cell at different cycles.

mechanism of action for high transference number electrolytes, those that reduce the rate of dendrite nucleation and growth should extend the short-circuit time for a given current density when compared to a bare electrode. In addition, the divergences in short-circuit time should increase with a higher current density, where cell polarization would be greatest.

To test this hypothesis, we polarized symmetric cells with PIM-coated lithium electrodes. Polarization was carried out at a current density of 0.5, 1.0, or 2.0 mA cm^{-2}. At the lowest current density, where the likelihood of differences in cell polarization due to transport bottlenecks is lowest, we found that the short-circuit times were similar for both symmetric cells, with PIM-coated electrodes providing a slight advantage: 270 h vs 223 h, respectively. However, advancing to a higher current density, where polarization is increasingly likely, the advantages of the rectifying PIM overlayer were clear and significant. When plated at 1 mA cm^{-2}, the symmetric cell configured with PIM-coated electrodes short-circuited within 39 h, which was nearly twice as long as the control cell (20 h). Similarly, when lithium metal was plated onto the Cu electrode at 2 mA cm^{-2}, the symmetric cell configured with PIM-coated electrodes short-circuited within 25 h, compared to 14 h for the control cell (Figure S1). Thus, at a high current density, the severe anion depletion causes a large space-charge field near the electrode−electrolyte interface, which gives rise to ramified growth of Li deposits and shorter short-circuit time for the cells. Due to the higher transference number possible using the nanostructured PIM overlayer, this space-charge effect is relaxed, and the short-circuit time extended by comparison.

Our insights thus far into the occurrence and propagation of lithium metal dendrites have not yet considered their impact on cell stability with respect to the electrolyte. The rate of parasitic side reactions between lithium metal and the electrolyte increases with an increasing surface area between them. From our Li−Li symmetric cell tests, the gradual decline in ASR over time was tied to an increase in surface area between the electrode and the electrolyte. Therefore, under- standing the impact of this morphological evolution in the system is critical. Electroanalytical determination of the Coulombic efficiency during sequences of plating and stripping in Li−Cu cells is a means to quantify the cycle-to-cycle prevalence of electrolyte degradation. We anticipated that cells configured with PIM overlayers would exhibit both a high Coulombic efficiency at a given current density, but also maintain it for a greater number of cycles when compared to control cells that do not feature the high cation transference number polymer overlayers.

To test this hypothesis, we reversibly plated Li metal on Cu electrodes in Li−Cu cells, in which the Cu electrodes were either coated with the PIM overlayer or left untreated (Figure 4A,B). Plating experiments were carried out at current densities of either 0.4 or 0.8 mA cm^{-2}, respectively, in 1 h durations. At the end of each plating step, a full strip of the Cu electrode was conducted, which was concomitant with a spike in the voltage. We calculated the Coulombic efficiency as the ratio of capacity stripped to the capacity plated in each cycle. Cells configured with PIM-coated electrodes exhibited higher Coulombic efficiencies and a longer cycle life at both current densities (Figures S2 and S3): for example, at 0.4 mA cm^{-2},

the Coulombic efficiency was >98% after 80 cycles, whereas it dropped precipitously after 60 cycles for the control cell. These data compare favorably to leading-edge work previously reported.[55−57] For cells cycling (Figure 4A) at 0.4 mAh cm^{-2}, the voltage profiles for both cells overlap in the first 60 cycles, after which the cell with untreated electrodes begins to lag. Interestingly, we found that the overpotentials for lithium metal plating were similar for both cells (~10 mV) at the lower current density (0.4 mA cm^{-2}) but differentiated at the higher current density (0.8 mA cm^{-2}), with observed values of 50 mV and 150 mV for PIM-coated and untreated electrodes, respectively (Figure 4B). While the origin of this may be due to differences in the rate of SEI formation between the two cell configurations, a more plausible explanation lies in the lower cell polarization at a high current density that is achieved using high cation transference number electrolytes.

Given the successes noted above in dendrite suppression at a high current density using PIM-coated lithium anodes, we endeavored further to demonstrate that these working principles were also efficacious in stabilizing lithium metal full cells relevant to electrified transportation. For this demonstration, we integrated the PIM-coated lithium anodes alongside an optimized high areal capacity sulfur cathode (4.9 mg cm^{-2}) that we have reported previously.[30] Briefly, the cathode confines the sulfur actives to *N*-doped mesoporous carbons (S@NMCs). These S@NMCs are cast along with a tailored polyelectrolyte binder, PEB-1, onto a current collector consisting of carbon nanofiber (CNF) paper. Li−S coin cells were assembled from these cathodes with a PIM-coated Li metal anode, a Celgard separator, and liquid electrolyte consisting of 1.0 M LiTFSI and 0.2 M $LiNO_3$ in 1:1 DOL/DME. The cells were cycled at 0.2 C, whereupon the accessible capacity remained constant at ~960 mAh g^{-1} (4.7 mAh cm^{-2}) after 120 cycles (Figure 4C,D). Additionally, this extended cycling resulted in a constant cell Coulombic close to 100%. These proof-of-concept demonstrations indicate that PIM-coated lithium metal electrodes are well-positioned to advance Li−S battery technology development, and potentially others implementing compatible cathode chemistries. Therefore, understanding their manufacturability may be of interest beyond these proof-of-concept demonstrations. While a solvent-based procedure has been used effectively to generate PIM-coated lithium electrodes for small-format coin cells, there may be manufacturing issues associated with coating reactive metals with flammable inks on a pilot line.

To map forward their manufacturing prospects for larger cell formats (e.g., pouch, cylindrical, prismatic), we considered alternative schemes that obviated the use of reactive or combustible solvents, yet had the potential to retain the conformal interface between lithium and polymer. We were ultimately successful in this endeavor using a pressure-driven lamination−delamination sequence. Here, PIM-1 was first coated to a desired thickness on a roll of mesoporous polypropylene (Celgard 2400). This construct was then applied directly onto lithium foil over a pressure range of 3.5−8.6 MPa using a static press. Subsequent peeling of the polyolefin resulted in complete transfer of the polymer onto lithium. Optical microscopy and SEM both showed that the polymer laminate was continuous, indicating a greater adhesion of PIM-1 to lithium than to the polyolefin support (Figure S4a). Transferred polymer overlayers exhibited a low density of pinholes. Those that persisted originated as defects in the initial PIM-1 coating on polypropylene, or where local

fracture initiates and propagates with separator peeling (Figure S4b). Such pinholes were not observed in pressure-laminated PIM-1, where the polyolefin support was removed through differential swelling in a suitable solvent (e.g., DME). In general, we found that the majority of the defects, while infrequent, were arc-shaped folds in the PIM-1, possibly induced by entrapped gas bubbles. Visualization of the exposed area where fracture jumped between the polyolefin support and lithium provided confirmation of intimate contact between PIM-1 and lithium (Figure S4b). For larger electrode formats, we used a battery electrode calendar to a similar effect.

The advantage of pressure-driven lamination is the ability to mate a freshly cleaned, reactive lithium surface with the protective polymer overlayer, avoiding reaction with carrier solvents, yielding a single anode−polymer−separator trilayer exhibiting a low area-specific resistance (ASR) for Li^+ transport when immersed in the LiTFSI-based DOL/DME electrolyte. We have accomplished pressure-lamination of PIM-1 and Li using commercially available roll stock with a roll press, demonstrating the possibility of precision fabrication of membrane-coated anodes to explore the PIM-1 attributes in anode protection and dendrite suppression at scale in larger cell formats and configurations.

The prevailing view from our work is that microporous polymer hosts[58] that rigidly enforce size restrictions at the nanometer-to-subnanometer scale to avoid excessive ion clustering in hybrid electrolytes can substantially increase the cation transference number, which can be leveraged to reduce electrode and cell polarization at high current densities. Doing so substantially delays the onset of dendrite formation and growth, instead allowing lithium metal to be reversibly plated uniformly and in dense morphologies. Maintaining a low interfacial area between lithium metal and the electrolyte is also advantageous in reducing parasitic side reactions that dry out the cell. With PIM-coated lithium anodes in place in energy-dense Li−S cells, we find stable cell performance even when implementing high capacity sulfur cathodes, which requires ~24 μm of lithium to be reversibly plated in each cycle. The stability of the anodes and associated cells in this regard is notable, considering advances elsewhere.[11] In addition, the scalability of the design appears to be amenable to larger cell formats without aggressively changing the design specifications. Similar strategies building on this work suggest exciting paths forward in macromolecular nanoionics to yield step changes in performance for critical battery components, from electrolytes to separators and binders, to make possible batteries that are both longer lasting and tailored for either fast charge or fast discharge, as needed for widespread electrified transportation.

AUTHOR INFORMATION

Corresponding Author
*E-mail: bahelms@lbl.gov.

ORCID
Kevin R. Zavadil: 0000-0002-3791-424X
Brett A. Helms: 0000-0003-3925-4174

Author Contributions
The manuscript was written through contributions of all authors. All authors have given approval to the final version of the manuscript.

Notes
The authors declare no competing financial interest.

ACKNOWLEDGMENTS

This work was supported by the Joint Center for Energy Storage Research (JCESR), an Energy Innovation Hub funded by the U.S. Department of Energy, Office of Science, Office of Basic Energy Sciences. Portions of this work, including polymer synthesis and characterization, were carried out as a user project at the Molecular Foundry, which is supported by the Office of Science, Office of Basic Energy Sciences of the U.S. Department of Energy under contract no. DE-AC02- 05CH11231. C.F. was supported by the Advanced Research Projects Agency-Energy Integration and Optimization of Novel Ion Conducting Solids (IONICS) program under grant no. DE-AR0000774 to carry out transport measurements on PIM- coated lithium metal electrodes. Z. Rostomian is thanked for assistance with the preparation of Figure [1],.

ABBREVIATIONS

PIM, polymer of intrinsic microporosity; PEB, polyelectrolyte binder; NMC, nitrogen-doped mesoporous carbon; DOL, 1,3- dioxolane; DME, 1,2-dimethoxyethane; LiTFSI, lithium bis-(trifluoromethanesulfonyl)imide; SEM, scanning electron microscopy; LPS, lithium phosphorus sulfide; LGPS, lithium germanium phosphorus sulfide; Li−S, lithium−sulfur; ASR, area-specific resistance

REFERENCES

(1) Schmuch, R.; Wagner, R.; Hörpel, G.; Placke, T.; Winter, M. *Nat. Energy* 2018, *3*, 267−278.
(2) Cano, Z. P.; Banham, D.; Ye, S.; Hintennach, A.; Lu, J.; Fowler, M.; Chen, Z. *Nat. Energy* 2018, *3*, 279−289.
(3) Zhao, Q.; Zheng, J.; Archer, L. A. *ACS Energy Lett.* 2018, *3*, 2104−2113.
(4) Sripad, S.; Viswanathan, V. *ACS Energy Lett.* 2017, *2*, 1669−1673.
(5) Sripad, S.; Viswanathan, V. *ACS Energy Lett.* 2019, *4*, 149−155.
(6) Fredericks, W. L.; Sripad, S.; Bower, G. C.; Viswanathan, V. *ACS Energy Lett.* 2018, *3*, 2989−2994.
(7) Choi, N.-S.; Chen, Z.; Freunberger, S. A.; Ji, X.; Sun, Y.-K.; Amine, K.; Yushin, G.; Nazar, L. F.; Cho, J.; Bruce, P. G. *Angew. Chem., Int. Ed.* 2012, *51*, 9994−10024.
(8) Choi, J. W.; Aurbach, D. *Nat. Rev. Mater.* 2016, *1*, 16013.
(9) Rosenman, A.; Markevich, E.; Salitra, G.; Aurbach, D.; Garsuch, A.; Chesneau, F. F. *Adv. Energy Mater.* 2015, *5*, 1500212.
(10) Lu, J.; Li, L.; Park, J.-B.; Sun, Y.-K.; Wu, F.; Amine, K. *Chem. Rev.* 2014, *114*, 5611−5640.
(11) Albertus, P.; Babinec, S.; Litzelman, S.; Newman, A. *Nat. Energy* 2018, *3*, 16−21.
(12) Lin, D.; Liu, Y.; Cui, Y. *Nat. Nanotechnol.* 2017, *12*, 194−206.
(13) Tikekar, M. D.; Choudhury, S.; Tu, Z.; Archer, L. A. *Nat. Energy* 2016, *1*, 16114.

(14) Xu, W.; Wang, J.; Ding, F.; Chen, X.; Nasybulin, E.; Zhang, Y.; Zhang, J.-G. *Energy Environ. Sci.* 2014, *7*, 513−537.
(15) Cheng, X.-B.; Zhang, R.; Zhao, C.-Z.; Zhang, Q. *Chem. Rev.* 2017, *117*, 10403−10473.
(16) Hong, Z.; Viswanathan, V. *ACS Energy Lett.* 2018, *3*, 1737−1743.
(17) Bruce, P. G.; Vincent, C. A. *J. Electroanal. Chem. Interfacial Electrochem.* 1987, *225*, 1−17.
(18) Evans, J.; Vincent, C. A.; Bruce, P. G. *Polymer* 1987, *28*, 2324−2328.
(19) Timachova, K.; Watanabe, H.; Balsara, N. P. *Macromolecules* 2015, *48*, 7882−7888.
(20) Monroe, C.; Newman, J. *J. Electrochem. Soc.* 2003, *150*, A1377−A1384.
(21) Lu, Y.; Tikekar, M.; Mohanty, R.; Hendrickson, K.; Ma, L.; Archer, L. A. *Adv. Energy Mater.* 2015, *5*, 1402073.
(22) Schaefer, J. L.; Yanga, D. A.; Archer, L. A. *Chem. Mater.* 2013, *25*, 834−839.
(23) Li, S.; Mohamed, A. I.; Pande, V.; Wang, H.; Cuthbert, J.; Pan, X.; He, H.; Wang, Z.; Viswanathan, V.; Whitacre, J. F.; Matyjaszewski, K. *ACS Energy Lett.* 2018, *3*, 20−27.
(24) Porcarelli, L.; Shaplov, A. S.; Bella, F.; Nair, J. R.; Mecerreyes, D.; Gerbaldi, C. *ACS Energy Lett.* 2016, *1*, 678−682.
(25) Morris, M. A.; An, H.; Lutkenhaus, J. L.; Epps, T. H. *ACS Energy Lett.* 2017, *2*, 1919−1936.
(26) Li, L.; Ma, L.; Helms, B. A. *Macromolecules* 2018, *51*, 7666−7671.
(27) Li, C.; Ward, A. L.; Doris, S. E.; Pascal, T. A.; Prendergast, D.; Helms, B. A. *Nano Lett.* 2015, *15*, 5724−5729.
(28) Suo, L.; Hu, Y.-S.; Li, H.; Armand, M.; Chen, L. *Nat. Commun.* 2013, *4*, 1481.
(29) Jorne, J. *Nano Lett.* 2006, *6*, 2973−2976.
(30) Li, L.; Pascal, T. A.; Connell, J. G.; Fan, F. Y.; Meckler, S. M.; Ma, L.; Chiang, Y.-M.; Prendergast, D.; Helms, B. A. *Nat. Commun.* 2017, *8*, 2277.
(31) Budd, P. M.; McKeown, N. B.; Ghanem, B. S.; Msayib, K. J.; Fritsch, D.; Starannikova, L.; Belov, N.; Sanfirova, O.; Yampolskii, Y.; Shantarovich, V. *J. Membr. Sci.* 2008, *325*, 851−860.
(32) Heuchel, M.; Fritsch, D.; Budd, P. M.; McKeown, N. B.; Hofmann, D. *J. Membr. Sci.* 2008, *318*, 84−99.
(33) Larsen, G. S.; Lin, P.; Hart, K. E.; Colina, C. M. *Macromolecules* 2011, *44*, 6944−6951.
(34) Doris, S. E.; Ward, A. L.; Frischmann, P. D.; Li, L.; Helms, B. A. *J. Mater. Chem. A* 2016, *4*, 16946−16952.
(35) Choudhury, S.; Agrawal, A.; Wei, S.; Jeng, E.; Archer, L. A. *Chem. Mater.* 2016, *28*, 2147−2157.
(36) Zhang, W.; Tu, Z.; Qian, J.; Choudhury, S.; Archer, L. A.; Lu, Y. *Small* 2018, *14*, 1703001.
(37) Popovic, J.; Hasegawa, G.; Moudrakovski, I.; Maier, J. *J. Mater. Chem. A* 2016, *4*, 7135−7140.
(38) Mistry, A.; Fear, C.; Carter, R.; Love, C. T.; Mukherjee, P. P. *ACS Energy Lett.* 2019, *4*, 156−162.
(39) Liu, J.; Wang, D.; Kvetny, M.; Brown, W.; Li, Y.; Wang, G. *Langmuir* 2013, *29*, 8743−8752.
(40) Liu, J.; Kvetny, M.; Feng, J.; Wang, D.; Wu, B.; Brown, W.; Wang, G. *Langmuir* 2012, *28*, 1588−1595.
(41) Feng, J.; Liu, J.; Wu, B.; Wang, G. *Anal. Chem.* 2010, *82*, 4520−4528.
(42) Li, Y.; Wang, D.; Kvetny, M. M.; Brown, W.; Liu, J.; Wang, G. *Chem. Sci.* 2015, *6*, 588−595.
(43) Cervera, J.; Ramírez, P.; Manzanares, J. A.; Mafé, S. *Microfluid. Nanofluid.* 2010, *9*, 41−53.
(44) Lu, Y.; Tu, Z.; Archer, L. A. *Nat. Mater.* 2014, *13*, 961−969.
(45) Tu, Z.; Choudhury, S.; Zachman, M. J.; Wei, S.; Zhang, K.; Kourkoutis, L. F.; Archer, L. A. *Joule* 2017, *1*, 394−406.
(46) Ding, F.; Xu, W.; Graff, G. L.; Zhang, J.; Sushko, M. L.; Chen, X.; Shao, Y.; Engelhard, M. H.; Nie, Z.; Xiao, J.; Liu, X.; Sushko, P. V.; Liu, J.; Zhang, J.-G. *J. Am. Chem. Soc.* 2013, *135*, 4450−4456.

(47) Zheng, J.; Engelhard, M. H.; Mei, D.; Jiao, S.; Polzin, B. J.; Zhang, J.-G.; Xu, W. *Nat. Energy* 2017, *2*, 17012.
(48) Ma, L.; Kim, M. S.; Archer, L. A. *Chem. Mater.* 2017, *29*, 4181−4189.
(49) Choudhury, S.; Tu, Z.; Stalin, S.; Vu, D.; Fawole, K.; Gunceler, D.; Sundararaman, R.; Archer, L. A. *Angew. Chem., Int. Ed.* 2017, *56*, 13070−13077.
(50) Bachman, J. C.; Muy, S.; Grimaud, A.; Chang, H.-H.; Pour, N.; Lux, S. F.; Paschos, O.; Maglia, F.; Lupart, S.; Lamp, P.; Giordano, L.; Shao-Horn, Y. *Chem. Rev.* 2016, *116*, 140−162.
(51) Manthiram, A.; Yu, X.; Wang, S. *Nat. Rev. Mater.* 2017, *2*, 16103.
(52) Zhang, Z.; Shao, Y.; Lotsch, B.; Hu, Y.-S.; Li, H.; Janek, J.; Nazar, L. F.; Nan, C.-W.; Maier, J.; Armand, M.; Chen, L. *Energy Environ. Sci.* 2018, *11*, 1945−1976.
(53) Bruce, P. G.; Evans, J.; Vincent, C. A. *Solid State Ionics* 1988, *28−30*, 918−922.
(54) Zheng, Q.; Ma, L.; Khurana, R.; Archer, L. A.; Coates, G. *Chem. Sci.* 2016, *7*, 6832−6838.
(55) Cheng, X.-B.; Hou, T.-Z.; Zhang, R.; Peng, H.-J.; Zhao, C.-Z.; Huang, J.-Q.; Zhang, Q. *Adv. Mater.* 2016, *28*, 2888−2895.
(56) Liu, W.; Lin, D.; Pei, A.; Cui, Y. *J. Am. Chem. Soc.* 2016, *138*, 15443−15450.
(57) Zhu, B.; Jin, Y.; Hu, X.; Zheng, Q.; Zhang, S.; Wang, Q.; Zhu, J. *Adv. Mater.* 2017, *29*, 1603755.
(58) Li, C.; Meckler, S. M.; Smith, Z. P.; Bachman, J. E.; Maserati, L.; Long, J. R.; Helms, B. A. *Adv. Mater.* 2018, *30*, 1704953.